Eur. Phys. J. D **38**, 523–532 (2006)
DOI: 10.1140/epjd/e2006-00049-7

THE EUROPEAN PHYSICAL JOURNAL D

Monte Carlo wavefunction approach to the dissipative quantum-phase dynamics of two-component Bose-Einstein condensates

M. Nakano[a], S. Ohta, R. Kishi, H. Takahashi, and S. Furukawa

Department of Materials Engineering Science, Graduate School of Engineering Science, Osaka University, Toyonaka, Osaka 560-8531, Japan

Received 6 October 2005 / Received in final form 2nd December 2005
Published online 14 March 2006 –

Abstract. We investigate the relaxation effects on the dynamics of two-component dilute gas Bose-Einstein condensates (BEC) with relatively different two-body interactions and Josephson couplings between the two components. Three types of relaxation effects, i.e., one- and three-body losses and a pure phase relaxation caused by elastic two-body collision between condensed and noncondensed atoms, are examined on the dynamical behavior of a macroscopic superposition, i.e., Schrödinger cat state, of two states with atom-number differences between the two components, which is known to be created by the time evolution in certain parameter regimes. Although three-body losses show a relatively large suppression of the revival behavior of Schrödinger cat state and the Pegg-Barnett phase-difference distribution between the two components for a small-size Schrödinger cat state, one- and three-body loss effects are not shown to directly depend on the size of Schrödinger cat state. In contrast, the pure-phase relaxation effects, causing a reduction of phase-difference distribution and then decaying the Schrödinger cat state, significantly increase with the increase of the size of Schrödinger cat state. These features suggest that a detection of damped collapse-revival behavior is highly possible for medium-size Schrödinger cat states in small-size two-component BECs.

PACS. 03.75.Gg Entanglement and decoherence in Bose-Einstein condensates – 03.75.Mn Multicomponent condensates; spinor condensates – 03.75.Kk Dynamic properties of condensates; collective and hydrodynamic excitations, superfluid flow – 03.67.Mn Entanglement production, characterization, and manipulation

1 Introduction

Recently, several proposals for the generation of meso-/macro-scopic quantum superposition states, i.e., Schrödinger cat states, in Bose-Einstein condensates (BECs) [1–3] have been reported [4–7]. The generation of Schrödinger cat states employs two-component BECs [8–11] composed of two hyperfine sublevels of ^{87}Rb, i.e., $|F, m_f\rangle = |1, -1\rangle$ and $|2, 2\rangle$ [8] or $|1, -1\rangle$ and $|2, 1\rangle$ [9–11], in which the two components can be coupled with each other via Josephson coupling achieved by the Raman or radio-frequency transitions. The generation scheme of Schrödinger cat state proposed by Gordon and Savage [6,7] uses a two component BEC with two-body interactions, i.e., atom-atom collisions, and weak Josephson coupling between the two components, where the interplay between the two-body interactions and the Josephson coupling leads to the Schrödinger cat states of the type by Cirac et al. [4]. The two- and four-mode models as well as a simple phase relaxation model are applied and predict the generation of Schrödinger cat states despite remaining limitations of these models [6]. In our previous paper [12], we have applied the Pegg-Barnett (PB) two-mode phase operators [13–19] to the investigation of the long-time behavior of Schrödinger cat state concerning two-component atom-number difference and relative phase dynamics of two-component BECs with various relative magnitude between the Josephson coupling and the difference between intra- and inter-component two-body interactions. In certain parameter regions, the created Schrödinger cat state turns out to exhibit collapse-revival behaviors in the long-time region, where the revival period, i.e. the lifetime of Schrödinger cat state, and its size, i.e., the interval between split two peaks of atom-number difference distribution, depend on the relative magnitude of these parameters.

Of course, such long-time collapse-revival behavior of Schrödinger cat state would be significantly suppressed by the dissipation and phase relaxation. In this study, we therefore investigate the effects of the loss of condensed

[a] e-mail: mnaka@cheng.es.osaka-u.ac.jp

atoms due to one- and three-body collisions [20,21] and the pure-phase relaxation due to the two-body collision between condensed and noncondensed atoms [7,22–24] on the dynamics of Schrödinger cat state concerning the atom-number difference between two components as well as the PB relative phase distribution. The characteristics of each relaxation effect are explored and discussed on their dependences on the size of Schrödinger cat state. Concerning the numerical calculation scheme of relaxation dynamics, the second-order Monte Carlo wavefunction (MCWF) approach [25] is formulated for the present model instead of conventional quantum master equation approach since the MCWF approach will be useful for the extended application to more complicated and large-size multi-component BEC systems though it is not necessary for the present application. The results obtained in the present study are important from the viewpoint of not only theoretical interests, e.g., how to relate the decoherence effects to the emergence of the macroscopically distinguishable states in the classical world from the superposition of different states in the quantum world [26–28], but also a measurement of meso/macro-scopic superposition states and the application to quantum information devices [29].

This paper is organized as follows. Section 2 contains a review of a model Hamiltonian for two-component BECs under the two-mode approximation as well as the Pegg-Barnett two-mode quantum-phase distribution. In Section 3, the quantum master equation involving one- and three-body losses and pure-phase relaxation is presented followed by its second-order Monte Carlo wavefunction unraveling scheme. Section 4 elucidates the dependence of long-time relaxation dynamics of atom-number difference on several relaxation parameters for two different sizes of Schrödinger cat states as well as the dynamics of phase-difference distribution between the two components. This is followed by a conclusion in Section 5.

2 Model Hamiltonian of two-component BECs and relative phase distribution

In this study, we consider a one-dimensional BEC system composed of two components (A and B). In the two-mode approximation, all modes except for the condensate modes, i.e., one mode for each component, are neglected. The Hamiltonian under this approximation becomes [6]

$$H_2 = E^A a^+ a + E^B b^+ b + \frac{\lambda}{2}\left(a^+ b + b^+ a\right) + \frac{W^{AA}}{2} a^+ a^+ a a + \frac{W^{BB}}{2} b^+ b^+ b\, b + W^{AB} a^+ b^+ b\, a, \tag{1}$$

where $E^{A(B)}$ is an energy of single particle Hamiltonian of component $A(B)$, W^{XY} is the two-body potentials describing collisions between condensed atoms of components X and Y, and λ is the strength of the Josephson coupling between the two components in the condensate mode. The system is described using the basis $|n_A, n_B\rangle$ ($n_A + n_B = N$ at the initial time, N is the total atom number), which is the product state of the number state with n_A atoms of component A and n_B atoms of component B. The energy standard is assumed to be set by $E^A = E^B = 0$. We also assume that the two intra-component two-body interaction coefficients are the same $W^{AA} = W^{BB} \equiv W$, which does not lead to any loss of generality in the two-mode approximation [6]. As an initial state, we consider the atomic coherent state [30,31] with phase difference ϕ between the two components:

$$|\Psi\rangle = \frac{1}{2^{N/2}\sqrt{N!}}\left(e^{i\phi} a^+ + b^+\right)^N |\mathrm{vac}\rangle = \frac{1}{2^{N/2}} \sum_{p=0}^{N} \sqrt{\binom{N}{p}} e^{i n_A \phi} |N, p\rangle\,. \tag{2}$$

The $\phi = 0$ state, which is created by applying $\pi/2$ pulse to N atoms in component A followed by a $\pi/2$ relative phase shift of the two components, is found to evolve into a Schrödinger cat state [6].

We here employ the two-mode Pegg-Barnett (PB) phase operator, which is used for evaluating the photon phase properties [12–19], in order to examine the relative phase (phase-difference, $\phi_B - \phi_A$) distribution between the two components of BECs. The two-component BECs $|\Psi\rangle$ are described in general:

$$|\Psi\rangle = \sum_{n_A, n_B} C_{n_A, n_B} |n_A, n_B\rangle, \tag{3}$$

where C_{n_A,n_B} is a coefficient and satisfies the condition: $n_A + n_B = N$ in the non-dissipative case. The corresponding density operator (ρ^{2BEC}) is written by

$$\rho^{2BEC} = |\Psi\rangle\langle\Psi| = \sum_{\substack{n_A, n_B \\ n'_A, n'_B}} C^*_{n'_A, n'_B} C_{n_A, n_B} |n_A, n_B\rangle\langle n'_A, n'_B|. \tag{4}$$

The two-mode PB phase distribution $P(\phi^A_{m_A}, \phi^B_{m_B})$, which represents the joint probability density for two-component phases $\phi^A_{m_A}$ and $\phi^B_{m_B}$, are expressed as

$$P(\phi^A_{m_A}, \phi^B_{m_B}) = \left|\left\langle \phi^A_{m_A}, \phi^B_{m_B} \middle| \Psi \right\rangle\right|^2 = \frac{1}{(s+1)^2} \sum_{\substack{n_A, n_B \\ n'_A, n'_B}} \rho^{2BEC}_{n_A, n_B, n'_A, n'_B} \times \exp i(n'_A - n_A)\phi^A_{m_A} \exp i(n'_B - n_B)\phi^B_{m_B}. \tag{5}$$

In equation (5), we use the following relation (6) between phase and number states in the one component case. In the PB approach, all calculations concerning the phase properties are performed in an $(s+1)$-dimensional space spanned by $s+1$ orthonormal phase states, in which s value is equal to the atom number N ($=n_A + n_B$) in the BEC. In the case of large s value, the $s+1$ phase states

become orthogonal with each other. The $s+1$ orthonormal phase states of a one-component BEC are defined by

$$|\phi_m\rangle = \frac{1}{(s+1)^{1/2}} \sum_{n=0}^{s} \exp(in\phi_m)\,|n\rangle, \tag{6}$$

where $\phi_m = \phi_0 + 2\pi m/(s+1)$ $(m = 0, 1, 2, ..., s)$ and ϕ_0 is an arbitrary real number. In this study, we adopt $\phi_0 = -s\pi/(s+1)$ to locate the initial phase of a one-component BEC on the origin ($\phi = 0$) of the phase axis defined in the region: $-\pi \le \phi_m \le \pi$. In the case of a two-component BEC, these relations are satisfied for each component. Using equation (5), the phase-difference distribution is given by

$$\begin{aligned} P(\phi^B_{m_B} - \phi^A_{m_A}) &\equiv P(\phi^-_m) \\ &= \frac{1}{s+1} \sum_{n_A, n_B} \sum_{n'_A} \rho^{2BEC}_{n_A, n_B, n'_A, n_A+n_B-n'_A} \\ &\quad \times \exp i(n_A - n'_A)\phi^-_m, \end{aligned} \tag{7}$$

which is turned out to be equal to $P(\phi^A_{m_A}, \phi^B_{m_B})$ (Eq. (5)) multiplied by $(s+1)$. This shows that the $P(\phi^A_{m_A}, \phi^B_{m_B})$ takes the same value on the line $\phi^B_{m_B} - \phi^A_{m_A} = \text{const.}$, which also leads to the fact that the phase-sum $P(\phi^A_{m_A} + \phi^B_{m_B})$ becomes a flat distribution, indicating the same probability for different phase-sum values. In general, the ϕ^-_m also has the 2π periodicity [14] and $P(\phi^-_m)$ is plotted in the region $-\pi \le \phi^-_m \le \pi$ with $\phi^-_m = (2m-s)\pi/(s+1)$. Although the relative phase operators are proposed and used for two-mode phase dynamics [32–36], we here employ the relative phase distribution generated by the absolute-phase approaches such as Pegg-Barnett since the positive operator valued measure (POVM) [32,34] generated by eigenstates of the relative phase operator is just the same induced by other absolute-phase approaches such as Pegg-Barnett, when cast to the appropriate 2π range.

3 Monte Carlo wavefunction approach to the dynamics of two-component BECs

3.1 Quantum master equation involving one- and three-body losses and pure-phase relaxation

In general, there are two kinds of relaxations for BECs, i.e., a population relaxation such as one- and three-body losses, and a pure-phase relaxation caused by the two-body collisions between condensed (trapped) and noncondensed (untrapped) atoms. We elucidate the effects of these relaxations on the long-time evolution of small- and large-size Schrödinger cat states. It is well-known that atomic losses of BECs are primarily caused by three-body losses, which represent the process that three atoms collide to form a biatomic molecule and an atom with large kinetic energy, followed by the escape of both of them from the trap. Another type of loss is one-body losses, in which individual atoms are dissipated from the trap due to the inelastic interaction with the thermal cloud of noncondensed atoms. Although the one-body losses can be reduced in principle in the case of a small number of noncondensed atoms with sufficient energy to kick atoms out of the trap, i.e., at sufficiently low temperatures, intrinsic three-body losses cannot be eliminated. The elastic two-body interaction between the condensed atoms and thermal cloud of noncondensed atoms causes a pure-phase relaxation, which becomes relatively important at low temperatures. Although the pure-phase relaxation effects on the creation of Schrödinger cat state have been examined in the previous study [7], the effects of one- and three-body losses as well as a pure relaxation on the collapse-revival behavior of Schrödinger cat state have not been investigated.

Using the previous results [7,22,37], deriving the analytical expression of decoherence time of BECs based on the quantum relaxation theory [38], the relaxation processes of the BECs are described effectively by the quantum master equation:

$$\dot{\rho} = i[\rho, H_2] + \mathcal{L}_{relax}\rho, \tag{8}$$

where

$$\mathcal{L}_{relax}\rho = (\mathcal{L}_{1body\text{-}loss} + \mathcal{L}_{3body\text{-}loss} + \mathcal{L}_{phase\text{-}rel})\rho. \tag{9}$$

The atomic unit ($\hbar = m_e = e = 1$) is used throughout this paper. Here, one- and three-body losses are expressed by

$$\begin{aligned} \mathcal{L}_{1body\text{-}loss}\rho = &\frac{\gamma_{1A}}{2}\left(2a\rho a^+ - a^+a\rho - \rho\, a^+a\right) \\ &+ \frac{\gamma_{1B}}{2}\left(2b\rho b^+ - b^+b\rho - \rho\, b^+b\right), \end{aligned} \tag{10}$$

and

$$\begin{aligned} \mathcal{L}_{3body\text{-}loss}\rho = &\\ &\frac{\gamma_{3A}}{2}\left[2\,(a)^3\,\rho\,\left(a^+\right)^3 - \left(a^+\right)^3\,(a)^3\,\rho - \rho\,\left(a^+\right)^3\,(a)^3\right] \\ &+ \frac{\gamma_{3B}}{2}\left[2\,(b)^3\,\rho\,\left(b^+\right)^3 - \left(b^+\right)^3\,(b)^3\,\rho - \rho\,\left(b^+\right)^3\,(b)^3\right], \end{aligned} \tag{11}$$

where γ_{nX} indicates the dissipation rate of BEC atoms for component X ($X = A$, B) by n-body losses. The pure-phase relaxation term is represented by

$$\begin{aligned} \mathcal{L}_{phase\text{-}loss}\rho = &\frac{\kappa_A}{2}\left[2n_A\rho n_A - (n_A)^2\rho - \rho(n_A)^2\right] \\ &+ \frac{\kappa_B}{2}\left[2n_B\rho n_B - (n_B)^2\rho - \rho(n_B)^2\right], \end{aligned} \tag{12}$$

where κ_X is a pure-phase relaxation rate for BEC component X ($X = A$, B), and n_X is the number operator for component X. It is noted that the pure-phase relaxation preserves the total number of condensed atoms composed of components A and B.

In this study, although these relaxation parameters are considered only from the viewpoint of the relative comparison of the effects of these relaxation processes on the

collapse-revival behavior of Schrödinger cat states, the explicit analytical forms for some of them are obtained as well as the details of derivation of the similar form of master equations in previous studies [7,22,37]. The relaxation parameter for three-body loss obtained by Jack [37] is expressed as

$$\gamma_3 \approx \tilde{\gamma}/3, \tag{13}$$

where $\tilde{\gamma}$ is a factor related to trap parameters, recombination rate K_3, etc. and gives a value of 3.3×10^{-12} s^{-1} for the BEC for ^{87}Rb with $N = 3 \times 10^5$ atoms with $K_3 = 2.2 \times 10^{-28}$ cm^6/s and trap parameters [37]. The three-body loss is caused by the three-body recombination process, which produces a molecule and an atom with a large kinetic energy and leads to the escape of them from the trap. This is considered to be a fundamental loss process because it cannot be reduced unlike the other loss caused by the collisions with untrapped (noncondensed) atoms. As mentioned in Section 4.2, the three-body loss effects scale as N^3, so that the it is more important for large-size BECs. Also, another type of three-body losses composed of two atoms of component $A(B)$ and one atom of component $B(A)$, which is not considered in this study, is estimated to give the same decoherence rate dependence (Eq. (31)) except for the case of large cat size ($m \sim N$), where the decoherence rate is significantly attenuated. We have estimated the dependence of the number of condensate similarly to the other relaxation cases. On the other hand, the one-body loss and pure-phase relaxations in this study are caused by the inelastic and elastic two-body collisions of condensed (trapped) atoms between noncondensed (untrapped) atoms, respectively [22]. Particularly, the relaxation rate by elastic two-body collisions, i.e., pure-phase relaxation, depends on the square of the size of Schrödinger cat (see Sect. 4.2) in contrast to the linear dependence for the rate by one-body loss, so that the elastic two-body collisions, leading to the pure-phase relaxation, are predicted to play a more important role on the relaxation of Schrödinger cat states. From the previous studies by Dalvit et al. [22] and Louis et al. [7], the pure-phase relaxation parameter κ is represented by

$$\kappa \approx 16\pi^3(8\pi a^2 n_{NC} v_T), \tag{14}$$

where a is a s-wave scattering length, n_{NC} is the number density of noncondensed atoms, and v_T ($=\sqrt{2k_BT/m}$) is their thermal velocity at temperature T. Using the values for ^{87}Rb ($a = 5$ nm and $m = 1.4 \times 10^{-25}$ kg) provides at $T = 1$ μK [7],

$$\kappa \approx 2 \times 10^{-15}\, n_{NC}. \tag{15}$$

The density of noncondensed atoms depends on temperature and typically ranges from 10^{19} m^3 just above the condensation temperature to zero at $T = 0$ [7]. It is noted that Dalvit et al. proposed an experimental scenario of dramatically reducing this type of relaxation thanks to trap engineering and symmetrization of the condensed atom cloud [22]. In Section 4, we estimate the decoherence time of Schrödinger cast state caused by three-body losses and pure-phase relaxation and discuss the possibility of experimental measurement of its collapse-revival behavior based on our results using model simulations and the above relation to experimental values.

3.2 Second-order Monte Carlo wavefunction approach

We briefly explain the calculation scheme of the second-order MCWF approach. In the quantum master equation, equation (8), the relaxation superoperator is represented by the Lindblad form [39] in the Born-Markov approximation [38] (see Eqs. (10–12)):

$$\mathcal{L}_{relax}\rho = -\frac{1}{2}\sum_m (C_m^+ C_m \rho + \rho C_m^+ C_m) + \sum_m C_m \rho C_m^+. \tag{16}$$

This type of relaxation operator is widely applied in dissipative dynamics in quantum optics, chemical physics, biology and so on. The Lindblad operators C_m^+ and C_m act on the system, and their forms depend on the nature of problem.

The original MCWF method simulates the evolution of quantum trajectories in Hilbert space conditioned on continuous detection of quanta, e.g., photons, involving two types of elements: smooth evolution by the non-Hermitian Hamiltonian H_{eff}, which originates in the first terms on the right-hand side of equations (8) and (16), and random interruptions of the non-Hermitian evolution by projections (quantum jumps) described by the second term on the right-hand side of equation (16). The higher-order unravelings in the MCWF method are advantageous to obtaining more accurate and stable numerical results [25]. In this study, the second-order unraveling method is employed. From the integration of the quantum master equation (8) to second order in δt, the following form is obtained [25]:

$$\begin{aligned}\rho(t+\delta t) &= U\rho(t)U^+ \\ &+ \frac{1}{2}\delta t \sum_m U C_m \rho(t) C_m^+ U^+ + \frac{1}{2}\delta t \sum_m C_m U \rho(t) U^+ C_m^+ \\ &+ \frac{1}{2}\delta t^2 \sum_{m,n} U C_m C_n \rho(t) C_n^+ C_m^+ U^+ + O(\delta t^3). \end{aligned} \tag{17}$$

Here, U indicates the non-Hermitian evolution, which is referred to as the "no-jump" evolution, under the influence of the effective Hamiltonian (Eq. (19)):

$$U = \exp\left(-iH_{\mathit{eff}}\delta t\right), \tag{18}$$

where

$$H_{\mathit{eff}} = H_2 - \frac{i}{2}\sum_m C_m^+ C_m. \tag{19}$$

The each term on the right-hand side of equation (17) represents the "minitrajectory" [25]. The density matrix evolution can be simulated with pure states by using an expansion of density matrix into minitrajectories. The first minitrajectory (the first term) of equation (17) ($m1$) describes a no-jump evolution, the second ($m2$) and third ($m3$) minitrajectories represent a jump followed by a

no-jump evolution and a no-jump evolution followed by a jump, respectively. The fourth minitrajectories ($m4$) describe two successive jumps followed by a no-jump evolution. It is noted that the second-order unraveling specifies two points: at the beginning and at the end of δt and requires two successive quantum jumps. The procedure of turning equation (17) into a Monte-Carlo simulation is obvious because each minitrajectory in equation (17) corresponds to the conditioned evolution of the system, which occurs with a specific probability. This procedure is described as follows. The normalized wavefunction $|\Psi(t+\delta t)\rangle$ of the BEC as well as the probability δp_l to choose its evolution in time step δt for each minitrajectory in equation (17) are represented by [40–42]

$$(m1) \quad |\Psi(t+\delta t)\rangle = \frac{U|\Psi(t)\rangle}{\sqrt{\delta p_1}}, \qquad \delta p_1 = \langle\Psi(t)|U^+U|\Psi(t)\rangle, \quad \text{(no jump)} \quad (20)$$

$$(m2) \quad |\Psi(t+\delta t)\rangle = \frac{UC_m|\Psi(t)\rangle}{\sqrt{\delta p_{2m}/(\delta t/2)}}, \qquad \delta p_{2m} = \langle\Psi(t)|C_m^+U^+UC_m|\Psi(t)\rangle\frac{\delta t}{2}, \quad (21)$$

$$(m3) \quad |\Psi(t+\delta t)\rangle = \frac{C_mU|\Psi(t)\rangle}{\sqrt{\delta p_{3m}/(\delta t/2)}}, \qquad \delta p_{3m} = \langle\Psi(t)|U^+C_m^+C_mU|\Psi(t)\rangle\frac{\delta t}{2}, \quad (22)$$

and

$$(m4) \quad |\Psi(t+\delta t)\rangle = \frac{UC_mC_n|\Psi(t)\rangle}{\sqrt{\delta p_{4m}/(\delta t^2/2)}}, \qquad \delta p_{4mn} = \langle\Psi(t)|C_n^+C_m^+U^+UC_mC_n|\Psi(t)\rangle\frac{\delta t^2}{2}. \quad (23)$$

In the second-order MCWF approach, we firstly generate a random number uniformly distributed between 0 and 1 in order to choose a minitrajectory (representing no-jump and/or jump evolutions of the system) with a specific probability in the next time step δt (see Eqs. (20–23)). The no-jump evolution is tested first because the probabilities choosing other minitrajectories (involving quantum jumps) are very small for small δt. If the no-jump minitrajectory is not chosen, one of the minitrajectories involving quantum jumps is chosen at the specific probability. After the evolution δt of wavefunction for a chosen minitarjectory, the resulting wavefunction is renormalized (see Eqs. (20–23)). Such procedure is repeated at each time step δt. Details of the numerical calculation procedure of the wavefunction at time $t+\delta t$ using the Monte Carlo method are presented in references [40–42].

After obtaining a sufficiently large number of trajectories $\rho^{(i)}(t)$ $\left(=\left|\Psi^{(i)}(t)\right\rangle\left\langle\Psi^{(i)}(t)\right|\right)$ constructed by the Monte Carlo wavefunctions $\left|\Psi^{(i)}(t)\right\rangle$, in which i indicates the trajectory number ($i = 1, ..., M_C$), we average these density matrix elements, $\langle n_A, n_B|\,\rho^{(i)}(t)\,|n'_A, n'_B\rangle$, at each time t using the basis of the two component BEC $\{|n_A, n_B\rangle\}$ spanned by the direct product of the number state of each component $\{|n_X\rangle\}$ ($n_X = 1, 2, ..., N_X$, $X = A, B$):

$$\rho_{n_A,n_B,n'_A,n'_B}(t) \equiv \langle n_A, n_B|\,\rho(t)\,|n'_A, n'_B\rangle \cong \frac{1}{M_C}\sum_{i=1}^{M_C}\langle n_A, n_B|\,\rho^{(i)}(t)\,|n'_A, n'_B\rangle. \quad (24)$$

The matrix elements using atom-number difference basis $\{|m\rangle\}$ ($m = n_A - n_B$) are calculated by

$$\rho_{m,m'}(t) = \sum_{\substack{n_A,n_B,n'_A,n'_B \\ (n_A-n_B=m, \\ n'_A-n'_B=m')}} \rho_{n_A,n_B,n'_A,n'_B}(t). \quad (25)$$

Note that the atom-number difference m ($=n_A - n_B$) satisfies the condition: $-N \le m \le N$, and it varies in units of two. Various properties, e.g., phase-difference distribution (Eq. (7)), concerning BEC state can be calculated using these reduced density matrices.

As mentioned in Section 3.1, we consider three types of Lindblad-type relaxations, i.e., one-body losses (Eq. (10)), three-body losses (Eq. (11)) and a pure-phase relaxation (Eq. (12)), of the BECs. The explicit forms of Lindblad operators C_m in equation (16) for these relaxation processes are described as follows.

$$C_1 = \sqrt{\gamma_{1A}}a, \quad C_2 = \sqrt{\gamma_{1B}}b \quad \text{(one-body losses)}, \quad (26)$$

$$C_3 = \sqrt{\gamma_{3A}}a^3, \; C_4 = \sqrt{\gamma_{3B}}b^3 \quad \text{(three-body losses)}, \quad (27)$$

and

$$C_5 = \sqrt{\kappa_A}n_A, \quad C_6 = \sqrt{\kappa_B}n_B \quad \text{(pure-phase relaxation)}. \quad (28)$$

Using equations (18–23) with these Lindblad operators, we can perform the dissipative dynamics of two-component BECs by the second-order MCWF approach.

4 Relaxation dynamics of atom-number and phase differences for two-component BECs

4.1 Parameter dependence of dynamical behavior of Schrödinger cat state in the non-relaxation case

For convenience of the following discussion, we summarize the results obtained in previous studies [6,7,12] on the creation and time evolution of Schrödinger cat state concerning atom-number difference distribution for two-component BECs. Gordon and Savage [6] have found that a two-mode model of a two-component BEC with two-body interactions ($W - W^{AB} \neq 0$) and weak Josephson coupling between the two components evolve into a Schrödinger cat state which differs in the atom-number difference between the two components. The mechanism

generating the Schrödinger cat states is explained in the previous papers [6,7]. They have also found that the size of the Schrödinger cat state depends on the Josephson coupling parameter λ: the maximal size is realized for $\lambda = \lambda_c$, which is given by references [6,30]

$$\lambda_c = \frac{N}{4}(W - W^{AB}). \tag{29}$$

Louis et al. [7] have reported that the Schrödinger cat state by Gordon-Savage scheme is created after a short-time evolution (≈2 s) of the initial state for a set of parameters: $N = 30$, $\lambda = 0.3\ \mathrm{s}^{-1}$, $W = 1.2\ \mathrm{s}^{-1}$ and $W^{AB} = 0.935\ \mathrm{s}^{-1}$, which corresponds to the region, $\lambda < \lambda_c$ (=1.9875 s^{-1}).

In our previous study [12], we have investigated the long-time dynamics of the atom-number difference between the two components of the two-component BEC for different relative magnitude between the Josephson coupling and the difference between intra- and inter-component two-body interactions. The feature of dynamics is shown to be classified by relative magnitude between λ and λ_c. Except for the two limit conditions, $\lambda_c \ll \lambda$ and $\lambda_c \gg \lambda$, the state has been found to evolve into a mesoscopic superposition state, i.e., Schrödinger cat state, composed of two states with different atom-number differences (m and $-m$) between the two components. Further, the created Schrödinger cat state has turned out to exhibit collapse-revival behaviors in the long-time region, in which the revival period, i.e. the lifetime of Schrödinger cat state, and its size, i.e., the interval between split two peaks of $\rho_{m,m}(t)$, are shown to depend on the relative magnitude between λ and λ_c. Figure 1 shows the dynamics of atom-number difference distribution $\rho_{m,m}(m)$, where m is the atom-number difference $n_A - n_B$ ($-30 \le m \le 30$ for $N = 30$), up to $t = 10$ s as well as the phase-difference distribution $P(\phi^-)$ (Eq. (7)) between the two components in the region $-\pi \le \phi^- \le \pi$ for the Josephson coupling parameter, $\lambda = 0.3\ \mathrm{s}^{-1}$ ($<\lambda_c$) (Figs. 1(a-1) and 1(a-2)) and $\lambda = 1.9\ \mathrm{s}^{-1}$ ($\approx\lambda_c$) (Figs. 1(b-1) and 1(b-2)). The time evolution of the initial state with $\phi = 0$ (Eq. (2)) using Hamiltonian H_2 (Eq. (1)) is carried out by the sixth-order Runge-Kutta method with a time step $\Delta t = 1.25 \times 10^{-4}$ s. For $\lambda = 0.3\ \mathrm{s}^{-1}$, a single peak at the initial time partitions into two peaks around $m = \pm 10$ at $t = 2$ s as shown in the study by Louis et al. [7]. From the magnitude of the off-diagonal density matrix $|\rho_{m,-m}(t)|$ ($m = \pm 10$) at $t = 2$ s (see Fig. 1c in Ref. [12]), the condensate state is turned out to be a superposition of a state (20 atoms in component A and 10 atoms in component B) and a state (10 atoms in component A and 20 atoms in component B). As seen from Figure 1(a-2), the initial state exhibits a single sharp peak at $\phi^- = 0$ (see Eq. (2)). When the time evolution starts, the single peak of $P(\phi^-)$ begins to diffuse and broaden symmetrically with respect to $\phi^- = 0$ [6]. In the subsequent time evolution ($10\ \mathrm{s} \ge t \ge 2\ \mathrm{s}$) for $\lambda = 0.3\ \mathrm{s}^{-1}$, the breadth of $P(\phi^-)$ is gradually reduced and peaks grow up around $\phi^- = 0$ after 2.5 s. This leads to the feature that in the region $2\ \mathrm{s} \le t \le 4$ s, two sharp peaks of $\rho_{m,m}(t)$ at $t = 2$ s are reduced, while several small peaks with smaller split intervals and broad distributions around

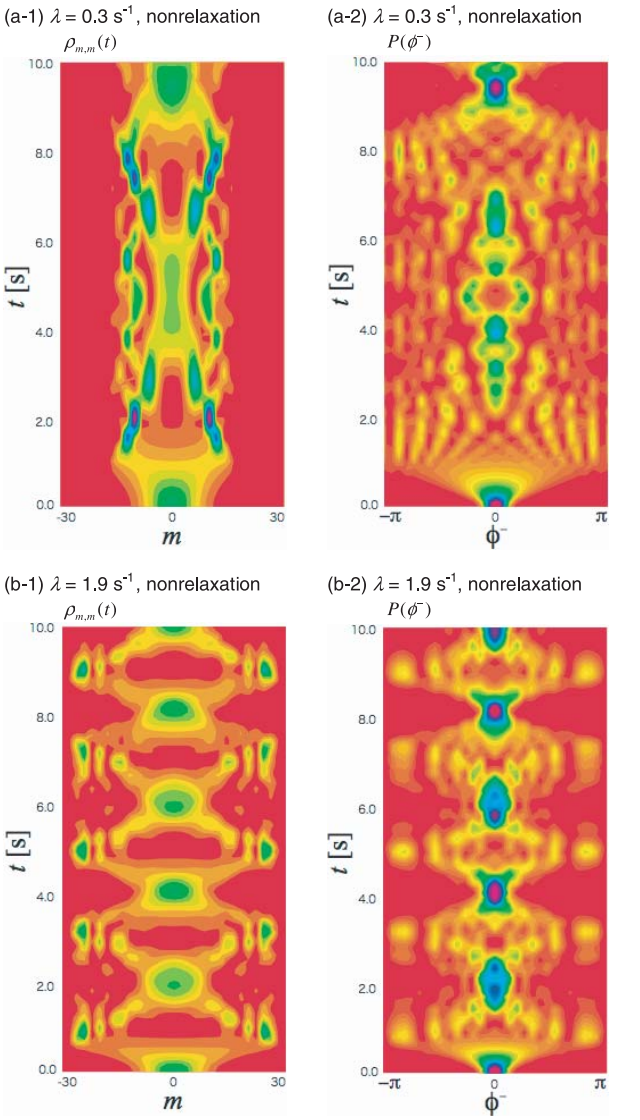

Fig. 1. Non-relaxation time evolutions of atom-number difference distribution $\rho_{m,m}(t)$ ($m = n_A - n_B$, $-30 \le m \le 30$ for $N = n_A + n_B = 30$) between components A and B from the initial state equation (2) for two types of parameters, $\lambda = 0.3\ \mathrm{s}^{-1}$, $W = 1.2\ \mathrm{s}^{-1}$ and $W^{AB} = 0.935\ \mathrm{s}^{-1}$ [(a-1)] and $\lambda = 1.9\ \mathrm{s}^{-1}$, $W = 1.2\ \mathrm{s}^{-1}$ and $W^{AB} = 0.935\ \mathrm{s}^{-1}$ [(b-1)], as well as their PB phase-difference distributions $P(\phi^-)$ ($\phi^- = \phi^B - \phi^A$) between the two components in the region $-\pi \le \phi^- \le \pi$ [(a-2) and (b-2)]. As the value increases, the color runs through red, yellow, green, cyan, blue, magenta, and back to red again. The number of contours is 40 for interval $(0.0, 0.4)$ for $\rho_{m,m}(t)$ and $P(\phi^-)$. A colour version is available in electronic form at `http://www.eurphysj.org`.

$\phi^- = 0$ grow up alternatively. Also, nearly symmetrical time-evolution behavior is observed in $\rho_{m,m}(t)$ and $P(\phi^-)$ with respect to $t = 4.5$ s in the region $0\ \mathrm{s} \le t \le 9$ s though the split and collision behaviors of these distributions are rather complicated. Although further long-time behavior is not shown in this study, nearly symmetrical repeating behavior of $P(\phi^-)$ and $\rho_{m,m}(t)$ are observed between the regions, $0\ \mathrm{s} \le t \le 9$ s and $9\ \mathrm{s} \le t \le 18$ s, indicating

a repeating period of about 9 s [12]. Such feature indicates the collapse-revival of Schrödinger cat state created at $t = 2$ s.

On the other hand, in the case of $\lambda = 1.9$ s^{-1}, which is nearly equal to λ_c and is expected to give the largest size of Schrödinger cat state (Figs. 1(b-1) and 1(b-2)): the atom number difference $|m|$ nearly amounts to the largest number 30 (the total atom number). As seen in our previous study [12], the collapse-revival period of the Schrödinger cat state is smaller (∼4 s) than that (∼9 s) for $\lambda = 0.3$ s^{-1} though the relation in the dynamical behavior between $\rho_{m,m}(t)$ and $P(\phi^-)$ is the same as that for $\lambda = 0.3$ s^{-1}. These results suggest that the repeating periods of revival structures are reduced when the Josephson coupling λ increases.

4.2 Effects of one- and three-body losses and a pure-phase relaxation on the dynamical behavior of Schrödinger cat state in the case of $\lambda = 0.3$ s^{-1} and $\lambda = 1.9$ s^{-1}

In this section, we examine the effect of dissipation, one- and three-body losses, and a pure-phase relaxation on the time evolution of Schrödinger cat state for two Josephson coupling cases: $\lambda = 0.3$ s^{-1} and $\lambda = 1.9$ s^{-1}. We assume that the three types of relaxation factors between two components are equal to each other, respectively, i.e., $\gamma_{1A} = \gamma_{1B} \equiv \gamma$, $\gamma_{3A} = \gamma_{3B} \equiv \gamma_3$ and $\kappa_A = \kappa_B \equiv \kappa$. We focus on the relative differences in the effects of these three types of relaxations by employing the relaxation factors nearly satisfying the realistic relative order of magnitudes [7,20–24]: $\gamma_1 = 1.0 \times 10^{-2}$ s^{-1}, $\gamma_3 = 3.0 \times 10^{-5}$ s^{-1} and $\kappa = 2.0 \times 10^{-2}$ s^{-1}.

Figure 2 shows the time evolutions of $\rho_{m,m}(t)$ and $P(\phi^-)$ for one-body losses, three-body losses and a pure-phase relaxation for the small-size Schrödinger cat state ($\lambda = 0.3$ s^{-1}). From Figures 2(a-1), 2(a-2), 2(b-1) and 2(b-2), one- and three-body losses give mutually similar tendencies of dissipation in $\rho_{m,m}(t)$ and dephasing in $P(\phi^-)$ though the relaxation factor of one-body losses is about 300 times as large as that of three-body losses. Namely, although the creation of Schrödinger cat state, i.e., two separate peaks of atom-number difference $[\rho_{m,m}(t)]$ around $m = \pm 10$, occurs around $t = 2$ s as well as the corresponding relative phase $[P(\phi^-)]$ diffusion as shown in non-relaxation case (Fig. 1), the subsequent behaviors of $\rho_{m,m}(t)$ and $P(\phi^-)$ are significantly damped and the revival behavior is hardly observed around $t =$ 9 s. The relaxation of phase-difference distribution is predicted to be caused by the phase relaxation originating in the one- and three-body losses. By contrast, the pure-phase relaxation (Figs. 2(c-1) and 2(c-2)), whose factor is two times as large as that of one-body losses, is turned out to less damp the atom-number difference distribution $[\rho_{m,m}(t)]$ than that for one-body losses, while the phase-difference distribution $[P(\phi^-)]$ is more significantly damped than those for one- and three-body losses. This shows that the creation of Schrödinger cat state and the subsequent time evolution are not significantly suffered

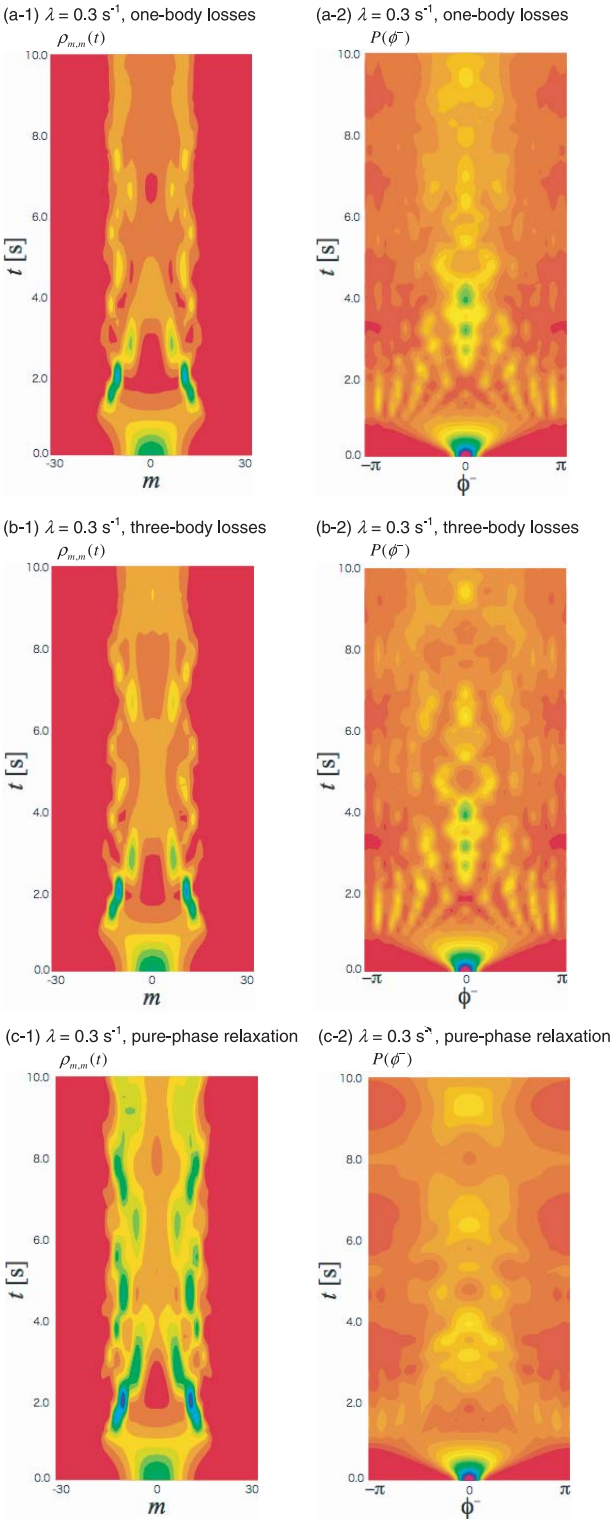

Fig. 2. Long-time evolution ($0 \leq t \leq 10$ s) of atom-number difference distribution $\rho_{m,m}(t)$ and phase-difference distribution $P(\phi^-)$ for small-size Schrödinger cat state ($\lambda = 0.3$ s^{-1}, $W = 1.2$ s^{-1} and $W^{AB} = 0.935$ s^{-1}) for one-body losses ($\gamma_1 = 1.0 \times 10^{-2}$ s^{-1}) [(a-1) and (a-2)], three-body losses ($\gamma_3 = 3.0 \times 10^{-5}$ s^{-1}) [(b-1) and (b-2)] and pure-phase relaxation ($\kappa = 2.0 \times 10^{-2}$ s^{-1}) [(c-1) and (c-2)]. See Figure 1 for further legends. A colour version is available in electronic form at `http://www.eurphysj.org`.

from the damped behavior of phase-difference distribution $[P(\phi^-)]$ in the case of small-size Schrödinger cat states. This can be understood by the fact that the phase diffusion, which is essential for creating Schrödinger cat state, sufficiently occurs in the present pure-phase relaxation rate and there is no direct dissipation of the number of atoms population in the case of pure-relaxation case.

For the large-size Schrödinger cat state ($\lambda = 1.9\ \mathrm{s}^{-1} \approx \lambda_c$), Figure 3 shows the time evolutions of $\rho_{m,m}(t)$ and $P(\phi^-)$ for one-body losses (Figs. 3(a-1) and 3(a-2)), three-body losses (Figs. 3(b-1) and 3(b-2)) and a pure-phase relaxation (Figs. 3(c-1) and 3(c-2)) with the same factors as those of $\lambda = 0.3\ \mathrm{s}^{-1}$ case. For atom-number difference distribution $\rho_{m,m}(t)$, the three-body losses cause slightly larger reduction of $\rho_{m,m}(t)$ and the size of Schrödinger cat state as the time proceeds compared to the case of one-body losses. Such difference in relaxation behaviors is more evident in the phase-difference $[P(\phi^-)]$ evolution (Fig. 3(a-2) vs. 3(b-2)): the $P(\phi^-)$ for three-body losses are more rapidly damped than that for one-body losses. This is in contrast to the case of the small-size Schrödinger cat state ($\lambda = 0.3\ \mathrm{s}^{-1}$), where one- and three-body losses give similar damping behaviors of $P(\phi^-)$ to each other (see Figs. 2(a-2) and 2(b-2)). The difference from the case of $\lambda = 0.3\ \mathrm{s}^{-1}$ more distinctively appears in the case of pure-phase relaxation. Namely, in the case of the large-size Schrödinger cat state, the degree of damping of $\rho_{m,m}(t)$ and $P(\phi^-)$ for pure-phase relaxation (Figs. 3(c-1) and 3(c-2)) is much larger than that for one- (Figs. 3(a-1) and 3(a-2)) and three- (Figs. 3(b-1) and 3(b-2)) body losses though in the case of small-size Schrödinger cat state the pure-phase relaxation gives somewhat less damped behavior of $\rho_{m,m}(t)$ (Fig. 2(c-1)) than the case of one- and three-body losses (Figs. 2(a-1) and 2(b-1)).

In order to understand the above difference in the effects of population (one- and three-body losses) and pure-phase relaxations between small- and large-size Schrödinger cat states, we consider the damping behaviors of a single-mode harmonic oscillator for these types of relaxations. From the master equation (Eq. (8)) with relaxation operators, equations (10–12), the off-diagonal density matrices at time t $[\rho_{m,-m}(t)]$ are approximately proportional to the initial $\rho_{m,-m}(0)$ except for their oscillatory behaviors:

$$\rho_{m,-m}(t) \propto \exp[-\gamma N t]\rho_{m,-m}(0), \quad \text{for one-body losses} \quad (30)$$

$$\rho_{m,-m}(t) \propto \exp[-\gamma N^3 t/4]\rho_{m,-m}(0), \quad \text{for three-body losses} \quad (m \ll N) \quad (31)$$

$$\rho_{m,-m}(t) \propto \exp[-\gamma N(N-1)(N-2)t]\rho_{m,-m}(0), \quad \text{for three-body losses } (m \approx N) \quad (32)$$

and

$$\rho_{m,-m}(t) \propto \exp[-\kappa m^2 t]\rho_{m,-m}(0), \quad \text{for pure-phase relaxation} \quad (33)$$

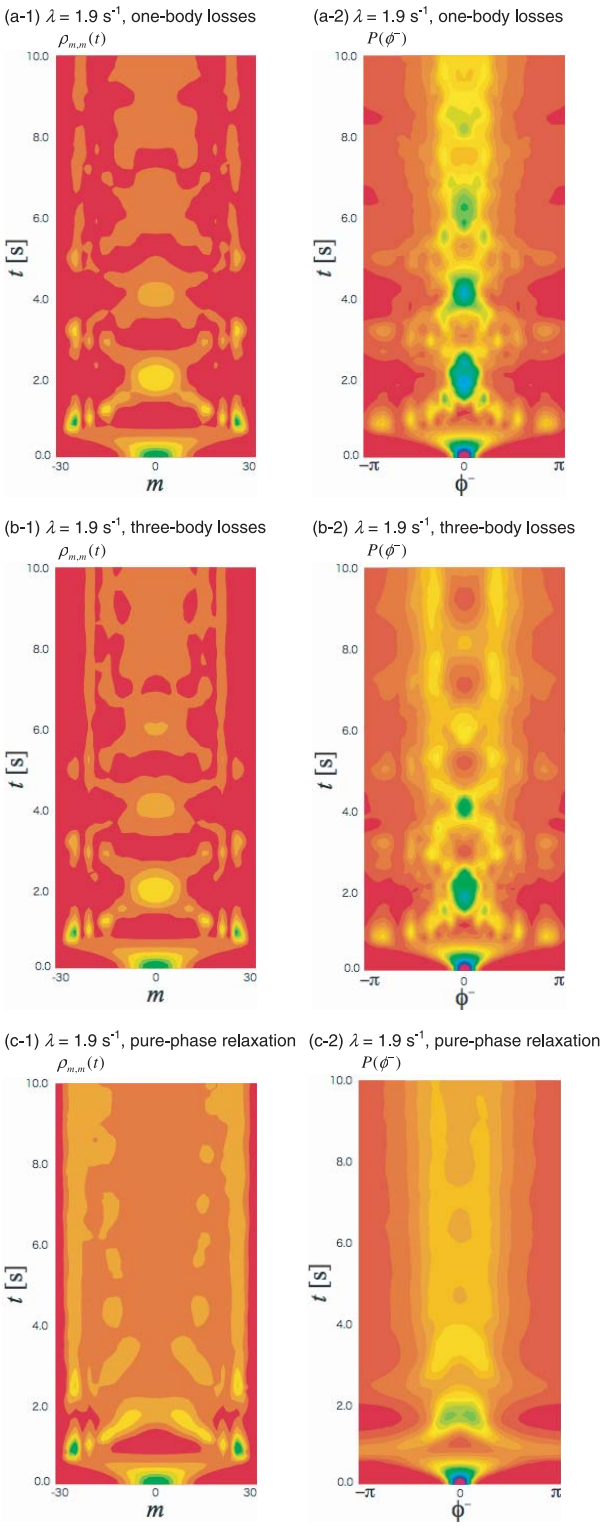

Fig. 3. Long-time evolution ($0 \le t \le 10$ s) of atom-number difference distribution $\rho_{m,m}(t)$ and phase-difference distribution $P(\phi^-)$ for large-size Schrödinger cat state ($\lambda = 1.9\ \mathrm{s}^{-1}$, $W = 1.2\ \mathrm{s}^{-1}$ and $W^{AB} = 0.935\ \mathrm{s}^{-1}$) for one-body losses ($\gamma_1 = 1.0 \times 10^{-2}\ \mathrm{s}^{-1}$) [(a-1) and (a-2)], three-body losses ($\gamma_3 = 3.0 \times 10^{-5}\ \mathrm{s}^{-1}$) [(b-1) and (b-2)] and pure-phase relaxation ($\kappa = 2.0 \times 10^{-2}\ \mathrm{s}^{-1}$) [(c-1) and (c-2)]. See Figure 1 for further legends. A colour version is available in electronic form at `http://www.eurphysj.org`.

where N and m depict the total number of atoms and the atom-number difference at the initial time, respectively. It is found from these approximate relations that the population relaxations (one- and three-body losses) give the relaxation rate depending on the total atom number ($\propto N$ for one-body losses and $\propto N^3$ for three-body losses), while the pure-phase relaxation gives the relaxation rate depending on the square of atom-number difference (m), i.e., the size of Schrödinger cat state [7]. Because the initial total number of atoms are constant ($N = 30$), this dependence supports the difference of relaxation effects between small ($m \approx 10$)- and large ($m \approx 30$)-size Schrödinger cat states (shown in Figs. 2 and 3): the pure-phase relaxation exhibits less damping effects for the small-size Schrödinger cat state ($\lambda = 0.3\ \mathrm{s}^{-1}$) than the population relaxations, while for the large-size Schrödinger cat state ($\lambda = 1.9\ \mathrm{s}^{-1}$) this tendency is reversed. The remarkable damping effects of three-body losses are understood by the fact that its relaxation rate is approximately proportional to N^3 in contrast to the relaxation rate for one-body losses, which is proportional to N. Also, the relaxation rate for three-body losses indirectly depends on the size of Schrödinger cat state (see Eqs. (31)) ($m \ll N$) and (32) ($m \approx N$)), which approximately indicates that the relaxation rate becomes larger in the largest-size Schrödinger cat states than in small-size Schrödinger cat states. This corresponds to the feature that for $\lambda = 1.9\ \mathrm{s}^{-1}$ ($m \approx N$) the three-body losses exhibit larger damped behaviors than one-body losses (see Figs. 3(a-2) and 3(b-2)), while for $\lambda = 0.3\ \mathrm{s}^{-1}$ one- and three-body losses exhibit similar damping effects to each other (see Figs. 2(a-2) and 2(b-2)).

In order to investigate the possibility of experimentally observing collapse and revival dynamics for a BEC, we estimate the Schrödinger cat state lifetime, i.e., decoherence time, for the three-body losses and pure-phase relaxation caused by elastic two-body collision between condensed (trapped) and noncondensed (untrapped) atoms using the approximate analytical formulae of relaxation parameters (Eqs. (13–15) in Sect. 3.1) obtained by previous studies [7, 22, 37] and our simulation results as well as the condensed atom number dependence of decoherence rate (Eqs. (30–33)). The decoherence time (τ_{3dec}) for three-body losses is estimated to be 4×10^{-5} s for ^{87}Rb ($N = 3 \times 10^5$) using equation (13) by Jack [37]. As predicted from the dependence of τ_{3dec} ($\tau_{3dec} \propto N^{-3}$) (Eq. (31)), the BEC with $N \sim 10^3$ is estimated to have the decoherence time with $\sim$10 s. On the other hand, the pure-phase decoherence caused by two-body collision between condensed (trapped) and noncondensed (untrapped) atoms is predicted to be important for large cat-size (the decoherence time dependence is $\tau_{dec} \propto m^{-2}$; m: cat size, Eq. (33)). From the present study with $N = 30$ and $m = 10$, the collapse-revival is predicted to occur within 10 s for $\lambda = 0.3\ \mathrm{s}^{-1}$. Dalvit et al. [22] have presented an approximate analytical expression of this type of pure-phase decoherence rate (Eq. (14)) and have shown that the decoherence rate also depends on n_{NC} (the density of noncondensed atoms), which depends strongly on temperature and typically ranges from $10^{19}\ \mathrm{m}^{-3}$ just above the condensation temperature to approximately 0 at $T = 0$ [7]. For ^{87}Rb case at $T = 1\ \mu$K considered in reference [3], decoherence time is approximately $\sim 10^{15}/(m^2 n_{NC})$. Therefore, if the n_{NC} is sufficiently small ($\sim 10^9$–$10^{10}\ \mathrm{m}^{-3}$), the decoherence time for $N = 3000$ and $m = 100$ is 10–100 s, which is expected to be larger than the collapse-revival period of $N = 30$ and $m = 10$ (see Fig. 1). Also, an extension of collapse-revival period up to that ($\sim$10 s) in the case of $N = 30$ and $m = 10$ will be feasible by tuning the Josephson coupling parameter λ. This suggests the possibility of observing the collapse-revival behavior of BEC though for larger size BEC system ($N \sim 10^5$–10^6) it will be hard to detect the collapse-revival behavior due to very small decoherence time caused by the three-body losses.

5 Conclusions

We have investigated the effects of three types of relaxations, i.e., one-body losses, three-body losses and a pure-phase relaxation, caused by the interaction with thermal clouds surrounding the BEC atoms and/or the collisions between condensed atoms, on the time evolution of atom-number difference Schrödinger cat state. Such Schrödinger cat state, which is created in the two-component BEC for different relative magnitude between the Josephson coupling and the difference between intra- and inter-component two-body interactions, is known to exhibit collapse-revival behavior in the long-time region in the case of non-relaxation. It is turned out that the three-body losses provide much larger damping effects of atom-number difference and phase-difference distributions than one-body losses though these losses are not significantly dependent on the size of Schrödinger cat state. In contrast, the pure-phase relaxation shows relatively smaller damping effects than one- and three-body losses in the case of small-size Schrödinger cat state, while pure-phase relaxation effects significantly enhance with the increase of the size of Schrödinger cat state. Using a single-mode harmonic oscillator model, we obtain the approximate dependence of each relaxation term on the total number of atoms and/or the size of Schrödinger cat state. Namely, the relaxation rate for one- and three-body losses are turned out to be approximately proportional to the total number of atoms (N) and N^3, respectively, while the pure-phase relaxation rate is proportional to the square of the size of Schrödinger cat state. From the present results, the one- and three-body losses are primary reasons of damping the creation and collapse-revival behavior of Schrödinger cat state for relatively small-size BECs, while the pure-phase relaxation dominates more significantly in such damping behavior as the size of Schrödinger cat state increases. Judging from the results that one- and three-body losses give relatively large effects for the small-size Schrödinger cat state, while the pure-phase relaxation more dominates in the large-size Schrödinger cat state, the generation of medium-size Schrödinger cat state by adjusting the Josephson coupling parameter will be highly possible for the experimental realization of Schrödinger cat state in relatively small two-component BECs ($N \sim 10^3$). Furthermore, from the result that

the collapse-revival period becomes smaller in larger-size Schrödinger cat state, the medium-size Schrödinger cat state will be also better for the detection of collapse-revival behavior of Schrödinger cat state during a relatively small period of time. Of course, we additionally have to require a reduction of the number density of non-condensed atoms to suppress the pure-phase relaxation and a sophisticated reservoir engineering to attenuate one-body losses.

This work was supported by Grant-in-Aid for Scientific Research (No. 14340184) from Japan Society for the Promotion of Science (JSPS).

References

1. M.H. Anderson, J.R. Ensher, M.R. Matthews, C.E. Wieman, E.A. Cornell, Science **269**, 198 (1995)
2. K.B. Davis, M.-O. Mewes, M.R. Andrews, N.J. van Druten, D.S. Durfee, D.M. Kurn, W. Ketterle, Phys. Rev. Lett. **75**, 3969 (1995)
3. C.C. Bradley, C.A. Sackett, J.J. Tollett, R.G. Hulet, Phys. Rev. Lett. **75**, 1687 (1995); C.C. Bradley, C.A. Sackett, R.G. Hulet, Phys. Rev. Lett. **78**, 985 (1997)
4. J.I. Cirac, M. Lewenstein, K. Mølmer, P. Zoller, Phys. Rev. A **57**, (1998) 1208
5. J. Rostekoski, M.J. Collet, R. Graham, D.F. Walls, Phys. Rev. A **57**, 511 (1998)
6. D. Gordon, C.M. Savage, Phys. Rev. A **59**, 4623 (1999)
7. P.J. Louis, P.M.R. Brydon, C.M. Savage, Phys. Rev. A **64**, 053613-1 (2001)
8. C.J. Myatt, E.A. Burt, R.W. Ghrist, E.A. Cornell, C.E. Wieman, Phys. Rev. Lett. **78**, 586 (1997)
9. M.R. Matthews, D.S. Hall, D.S. Jin, J.R. Ensher, C.E. Wieman, E.A. Cornell, F. Dalfovo, C. Minniti, S. Stringari, Phys. Rev. Lett. **81**, 243 (1998)
10. D.S. Hall, M.R. Matthews, J.R. Ensher, C.E. Wieman, E.A. Cornell, Phys. Rev. Lett. **81**, 1539 (1998)
11. D.S. Hall, M.R. Matthews, C.E. Wieman, E.A. Cornell, Phys. Rev. Lett. **81**, 1543 (1998)
12. M. Nakano, R. Kishi, S. Ohta, H. Takahashi, S. Furukawa, K. Yamaguchi, Physica B **370**, 110 (2005)
13. S.M. Barnett, D.T. Pegg, J. Mod. Opt. **44**, 225 (1997)
14. S.M. Barnett, D.T. Pegg, Phys. Rev. A **42**, 6713 (1990)
15. M. Nakano, K. Yamaguchi, Phys. Rev. A **64**, 033415-1 (2001)
16. M. Nakano, K. Yamaguchi, J. Chem. Phys. **116**, 10069 (2002)
17. M. Nakano, K. Yamaguchi, J. Chem. Phys. **117**, 9671 (2002)
18. M. Nakano, K. Yamaguchi, Chem. Phys. **286**, 257 (2003)
19. M. Nakano, K. Yamaguchi, Int. J. Quant. Chem. **99**, 421 (2004)
20. W. Ketterle, in Bose-Einstein Condensation in Atom Gases, *Proceedings of the International School of Physics "Enrico Fermi"*, Course 140, edited by M. Inguscio, S. Stringari, C. Wieman (IOS Press, Amsterdam, 1999)
21. J. Dziarmaga, K. Sacha, Phys. Rev. A **68**, 043607 (2003)
22. D.A.R. Dalvit, J. Dziarmaga, W.H. Zurek, Phys. Rev. A **62**, 013607 (2000); `arXiv:cond-mat/0006349` (2000)
23. J. Anglin, Phys. Rev. Lett. **79**, 6 (1997)
24. J. Ruostekoski, D.F. Walls, Phys. Rev. A **58**, R50 (1998)
25. J. Steinbach, B.M. Garraway, P.L. Knight, Phys. Rev. A **51**, 3302 (1995)
26. A.J. Leggett, A. Garg, Phys. Rev. Lett. **54**, 857 (1985)
27. E. Schrödinger, Naturwissenschaften **23**, 807 (1935); E. Schrödinger, Naturwissenschaften **23**, 823 (1935); E. Schrödinger, Naturwissenschaften **23**, 844 (1935)
28. *Quantum Theory and Measurement*, edited by J.A. Wheeler, W.H. Zurek (Princeton University Press, Princeton, NJ, 1983)
29. *The Physics of Quantum Information: Quantum Cryptography, Quantum Teleportation, Quantum Computation*, edited by D. Bouwmeester, A. Ekert, A. Zeilinger (Springer, Berlin, 2000)
30. G.J. Milburn, J. Corney, E.M. Wright, D.F. Walls, Phys. Rev. A **55**, 4318 (1997)
31. F.T. Arrechi, E. Courtens, R. Gilmore, H. Thomas, Phys. Rev. A **6**, 2211 (1972)
32. A. Luis, L.L. Sánchez-Soto, Phys. Rev. A **48**, 4702 (1993)
33. Y. Yang, W. Feng, X. Wu, Mod. Phys. Lett. A **12**, 2141 (1997)
34. J. Delgado, E.C. Yustas, L.L. Sánchez-Soto, A.B. Klimov, Phys. Rev. A **63**, 063801 (2001)
35. J. Javanaine, M. Wilkens, Phys. Rev. Lett. **78**, 4675 (1997)
36. J. Javanaine, M. Wilkens, Phys. Rev. A **60**, 2351 (1999)
37. M. Jack, Phys. Rev. Lett. **89**, 140402 (2002)
38. H.J. Carmichael, *Statistical Methods in Quantum Optics 1. Master equations and Fokker-Plank Equations* (Springer, Berlin, 1999)
39. G. Lindblad, Commun. Math. Phys. **48**, 119 (1976)
40. M. Nakano, K. Yamaguchi, Int. J. Quant. Chem. **95**, 461 (2003)
41. M. Nakano, R. Kishi, T. Nitta, K. Yamaguchi, J. Chem. Phys. **119**, 12106 (2003)
42. M. Nakano, R. Kishi, T. Nitta, K. Yamaguchi, Phys. Rev. A **70**, 033407-1 (2004)